Article

Preparation and Characterization of GaN-on-Si HEMTs with Nanocrystalline Diamond Passivation

Yu Fu [1], Songyuan Song [1], Zeyang Ren [1,2,*], Liaoliang Zhu [1,2], Jinfeng Zhang [1,2,*], Kai Su [1], Junfei Chen [1,2], Tao Zhang [1], Weidong Zhu [1], Junpeng Li [2], Weidong Man [3], Yue Hao [1] and Jincheng Zhang [1,*]

[1] State Key Laboratory of Wide-Bandgap Semiconductor Devices and Integrated Technology, Xidian University, Xi'an 710071, China; fuyu@xidian.edu.cn (Y.F.); 23111213659@stu.xidian.edu.cn (S.S.); 21111213027@stu.xidian.edu.cn (L.Z.); ksu@xidian.edu.cn (K.S.); chenjunfei@xdwh-inst.com (J.C.); zhangtao@xidian.edu.cn (T.Z.); wdzhu@xidian.edu.cn (W.Z.); yhao@xidian.edu.cn (Y.H.)

[2] Xidian-Wuhu Research Institute, Wuhu 241002, China; jpli_xidian@163.com

[3] Shanghai Zhengshi Technology Co., Ltd., Shanghai 201799, China

* Correspondence: zeyangren@xidian.edu.cn (Z.R.); jfzhang@xidian.edu.cn (J.Z.); jchzhang@xidian.edu.cn (J.Z.)

Abstract: Thermal accumulation under high output power densities is one of the most significant challenges for GaN power devices. Diamond, with its ultra-high thermal conductivity, offers great potential for improving heat dissipation in high-power GaN devices. In this study, nanocrystalline diamond (NCD) passivated high-electron mobility transistors (HEMTs) based on AlGaN/GaN-on-Si heterostructures were fabricated with a gate length of 2 µm. The NCD film has a thickness of 250–383 nm and a uniform morphology with a grain size of mostly ~240 nm. Compared to the devices without NCD passivation, those devices with the NCD passivation layer show an increase in current density from 447 mA/mm to 555 mA/mm, a reduction in on-resistance from 20 Ω·mm to 13 Ω·mm, and a noticeable suppression of current degradation at high-drain voltages. Junction temperature measurements under varied output power densities reveal a 36% improvement in heat dissipation efficiency with the NCD passivation. These results fully demonstrate the promising potential of NCD for enhancing heat dissipation in high-power GaN devices.

Keywords: nanocrystalline diamond; GaN; HEMT; heat dissipation

Academic Editor: Zongyou Yin

Received: 27 January 2025
Revised: 22 February 2025
Accepted: 27 February 2025
Published: 28 February 2025

Citation: Fu, Y.; Song, S.; Ren, Z.; Zhu, L.; Zhang, J.; Su, K.; Chen, J.; Zhang, T.; Zhu, W.; Li, J.; et al. Preparation and Characterization of GaN-on-Si HEMTs with Nanocrystalline Diamond Passivation. *Crystals* **2025**, *15*, 242. https://doi.org/10.3390/cryst15030242

Copyright: © 2025 by the authors. Licensee MDPI, Basel, Switzerland. This article is an open access article distributed under the terms and conditions of the Creative Commons Attribution (CC BY) license (https://creativecommons.org/licenses/by/4.0/).

1. Introduction

Gallium nitride offers significant advantages in high-frequency, high-power, and high-temperature applications due to its large bandgap and high carrier mobility [1–4]. GaN material has wide applications in radar, communication modules, wireless energy transmission [1,5], and high-efficiency power converters [6,7]. Effective heat dissipation becomes crucial when GaN devices operate at high power densities [8–11]. Without efficient thermal management, heat accumulation can cause a sharp increase in junction temperature, leading to reduced output power density and efficiency. While various strategies aiming at high-efficiency heat dissipation at the packaging level have been explored [11], further research is also needed at the device level to prevent hotspot buildup and to rapidly dissipate heat from the active region [12].

Diamond, with the highest thermal conductivity in nature, holds great promise for improving heat dissipation in GaN-based devices [12]. The thermal conductivity of single-crystalline diamond can exceed 2000 W/(m·K) [8], approximately five times that of SiC. For nanocrystalline diamond, its thermal conductivity ranges from 20 to 200 W/m·K

depending on the thickness and grain sizes [13]. Currently, epitaxial layers of GaN HEMTs are typically grown on substrates like SiC, Si, and sapphire. For the GaN HEMTs operating in large power operations, these materials cannot meet the increasing demands to efficiently conduct heat away from the hotspot or rapidly cool the junction [14]. Replacing existing substrates with diamond, either by bonding or heteroepitaxial growth, has been widely studied [15–21]. However, direct bonding of polycrystalline diamond and GaN is very challenging due to the large difficulty in fine diamond surface polishing and wafer-scale chemical bonding between diamond and GaN materials [22]. Most studies regarding GaN-on-diamond bonding involve the introduction of interlayers [20], but these interlayers can introduce additional thermal boundary resistance (TBR) [19,23,24]. Heteroepitaxial growth of polycrystalline diamond on the back of GaN wafers as a heat sink is also challenging due to the harsh diamond growth environment, which can degrade the nitride materials [25]. Furthermore, the large lattice and thermal mismatch between GaN and diamond leads to significant stress.

An alternative solution to using diamond to dissipate heat is to grow a nanocrystalline diamond passivation layer above the active regions of the devices [26–28]. This approach facilitates very rapid heat extraction from the hotspot due to placing the diamond heat dissipation layer at a nanoscale adjacent to the junction [28,29]. The low growth temperature and short growth time of the NCD passivation layer ensure minimal degradation of the AlGaN surface and the heterojunction [30]. Moreover, this strategy is compatible with existing GaN device fabrication processes. However, the existing method faces the problem of high NCD growth temperatures. In previous studies, the NCD growth temperature reached up to 750 °C [27,31], while the high-temperature hydrogen plasma would have a strong destructive effect on GaN [32].

In this study, we grew a NCD passivation layer on Si-based GaN HEMTs by microwave plasma chemical vapor deposition (MPCVD) at a low temperature of 650 °C. A comparison is made between the device characteristics with and without NCD passivation. The NCD-passivated devices exhibited better output DC characteristics and heat dissipation performances, demonstrating the promising prospect of using NCD passivation layers in GaN high-power devices.

2. Experiments

In this study, a home-made 4-inch AlGaN/GaN-on-Si wafer cutting into 1.5 × 1.5 cm^2 pieces was used. The epi-structure consisted of a 20 nm $Al_{0.21}Ga_{0.79}N$ barrier layer, a 190 nm GaN channel layer and a 4.49-µm GaN buffer layer. The device fabrication process is illustrated in Figure 1. To avoid the possible failure of the Schottky gate due to the NCD growth at 650 °C, we employed the strategy with the NCD growth before the gate preparation of the device.

Before device fabrication, the sample was thoroughly cleaned to remove any contaminants from the surface. Chlorine-based dry etching was then performed to create mesa isolation between the devices. Following this, electron beam evaporation was used to deposit a Ti/Al/Ni/Au multilayer stack with thicknesses of 20/150/50/100 nm to form the source and drain electrodes. The sample was then placed in an Annealsys rapid thermal annealing (RTA) system (AS-One150) at 835 °C for 30 s in a pure N_2 atmosphere to achieve the ohmic contact.

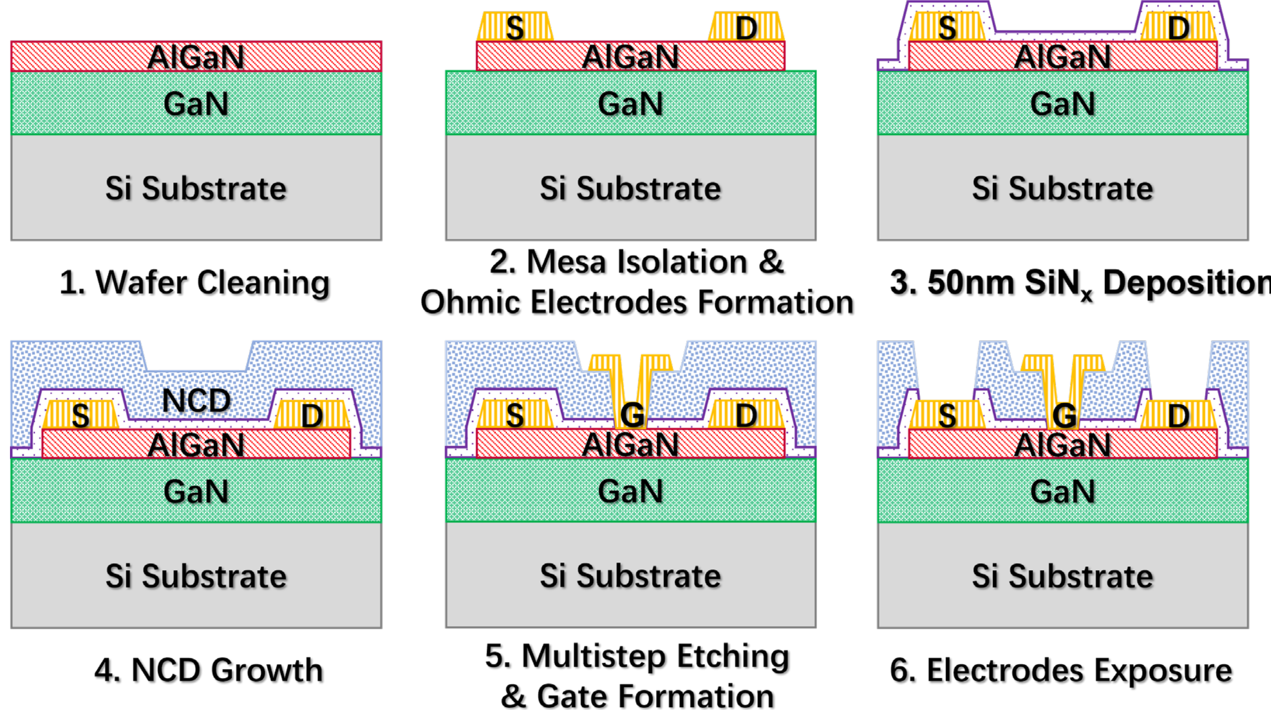

Figure 1. Schematic diagram of the fabrication processes of the NCD passivated GaN HEMTs.

Next, a 50 nm-thick SiN_x protection layer was deposited at 130 °C using SENTECH SI500D inductively coupled plasma chemical vapor deposition (ICP-CVD) to protect the AlGaN/GaN material during the NCD growth process. Afterwards, we spin-coated the nanocrystalline diamond seed suspension onto the sample surface at 2000 rpm for 30 s, followed by drying the sample at 80 °C to complete the seeding. NCD film was then grown using a two-step strategy in a MPCVD system from the Worldiray company. The gas flow rates were 300 sccm for H_2, 12 sccm for CH_4, and 0.05 sccm for N_2. The gas flow rates remain unchanged during the whole NCD growth process. Initially, nucleation growth was performed for 120 s under low-power conditions (2.0 kW and 90 mbar) to form a thin membrane for preventing the etching of the sample surface by hydrogen plasma. The main growth was then carried out for 15 min to thicken the NCD film and enlarge the grains, with the microwave power and pressure set to 3.2 kW and at 135 mbar, respectively.

Following the NCD growth, a 200 nm-thick SiN_x hard mask was deposited by ICP-CVD, and the SiN_x hard mask was then selectively etched by ICP in CF_4 atmosphere under 300W ICP power, 50W RF power for 90 s to expose the gate area covered by NCD. The exposed NCD was then removed by oxygen plasma etching. Finally, the gate metal (Ni/Au, with thicknesses of 20/200 nm) was deposited, followed by a lift-off process to complete the device fabrication. To facilitate subsequent testing, the NCD and SiN_x layers that covering the source and drain electrodes were removed using the aforementioned etching method. The scanning electron microscope (SEM) images of the prepared devices are shown in Figure 2.

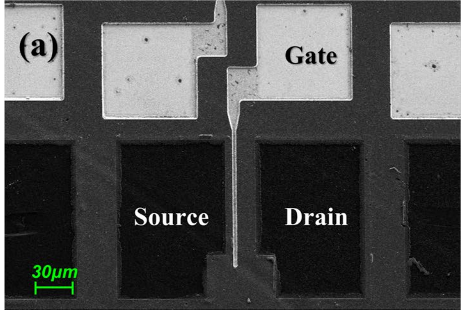

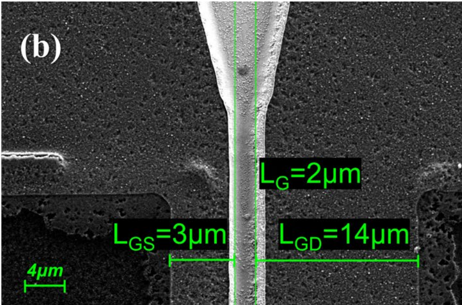

Figure 2. SEM micrographs of the fabricated devices. (**a**) Overview of the HEMT device with NCD passivation; (**b**) magnified view of the local 2 μm-gate region area.

A KEYSIGHT B1500A semiconductor parameter analyzer was used to measure the DC characteristics as well as the influence of NCD growth on the ohmic contact of the devices. Additionally, the junction temperatures of devices with and without the NCD passivation layer were simultaneously recorded under varying DC power levels. All tests were conducted at room temperature.

3. Results and Discussion

As shown in Figure 3a, SEM images of the sample after NCD passivation show that the NCD grain sizes are primarily around 240 nm, indicating good in-plane uniformity of the growth. The total thickness of the grown NCD layer is 250–383 nm (Figure 3b).

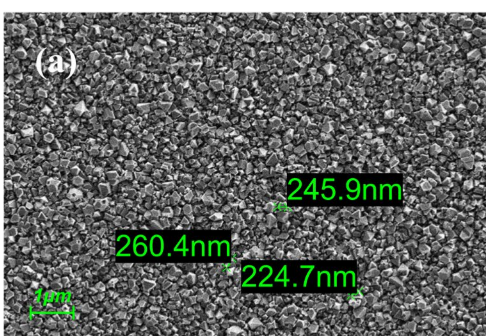

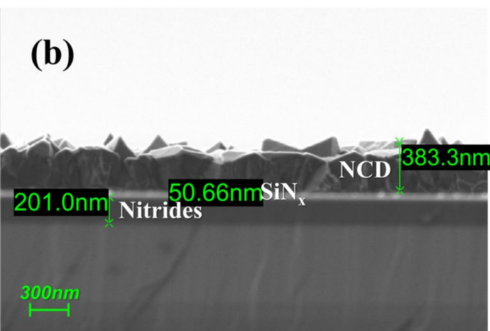

Figure 3. SEM micrographs of the sample after NCD film growth. (**a**) Surface morphology and (**b**) cross-section view.

To further characterize the properties of the NCD films, a WITec alpha300RS system was used to perform Raman spectroscopy on the samples. The laser wavelength was 532 nm, and the grating had 600 grooves/mm. As shown in Figure 4, the peak that corresponding to diamond and locating at near 1333 cm^{-1} is clearly observed, confirming the successful growth of a uniform NCD film [33]. Additionally, the presence of trans-polyacetylene (TPA) peaks near 1140 cm^{-1} and 1490 cm^{-1} can be attributed to non-diamond phases, which are commonly observed in the NCD growth [34]. In future studies, by optimizing the growth condition, the quality of diamond can be improved [35]. For instance, by reducing the CH_4 flow while maintaining the H_2 flow, the etching of non-diamond phases by H plasma is enhanced, which can not only improve the quality of the diamond but also lead to a slower growth rate. The absence of noticeable graphite-related peaks between 1500 and 1600 cm^{-1} indicates a low graphite content, making it possible that a high thermal conductivity can be obtained in the passivation layer [13].

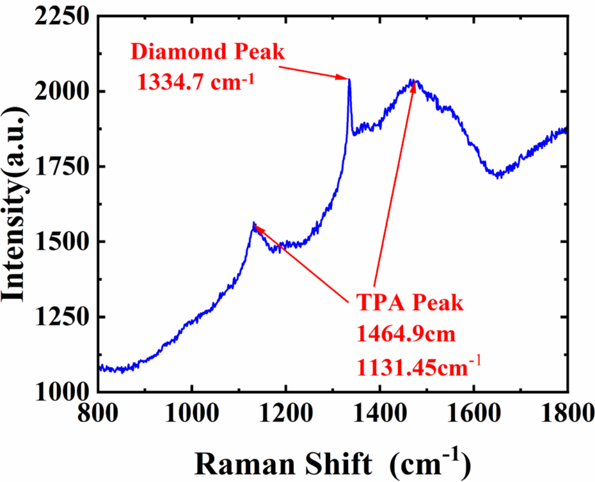

Figure 4. Raman spectrum on the AlGaN/GaN-on-Si sample after NCD growth.

To investigate the changes in the AlGaN/GaN epi-film before and after NCD growth, X-ray diffraction (XRD) measurements were carried out by an X'Pert MRD facility. The rocking curves for the (002) and (102) planes of the GaN layer are shown in Figure 5. After NCD growth, the full width at half maximum (FWHM) of the (002) curve slightly decreases (492 arcsec to 481 arcsec) along with the maximum intensity increase for 5000 counts. The FWHM of the (102) curve increases from 754 arcsec to 798 arcsec, and the maximum intensity nearly remains unchanged. The XRD results show that the growth of NCD induces an acceptable change in GaN quality that differs from the (002) to (102) plane. In general, the 50 nm-thick SiN_x layer effectively protects the AlGaN/GaN heterojunction from remarkable degradation that could result from the harsh conditions during NCD growth.

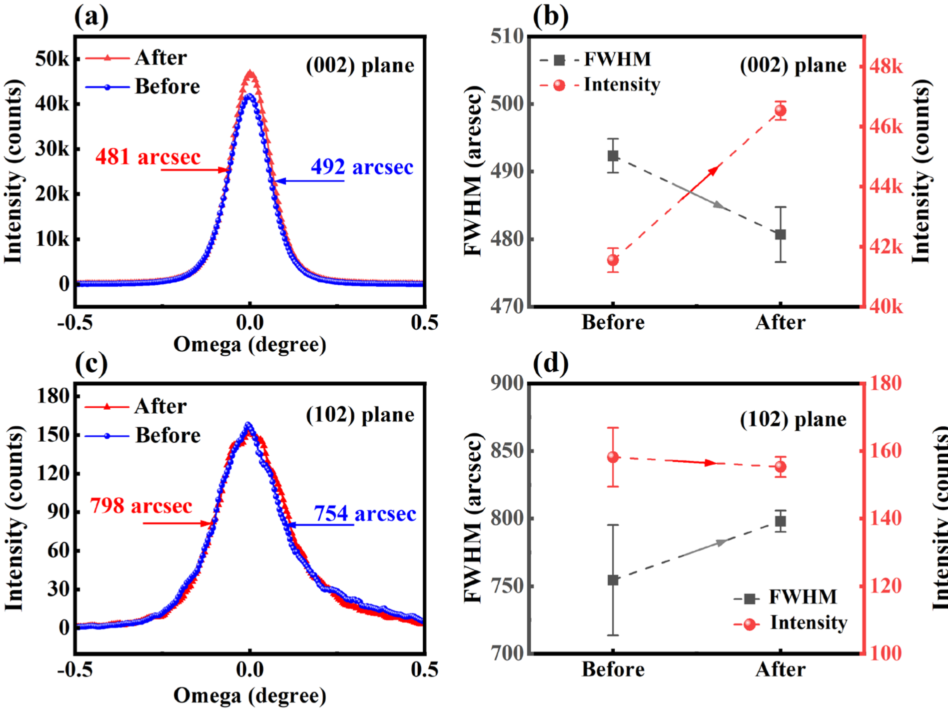

Figure 5. X-ray diffraction results of the prepared sample before and after NCD growth. (**a**) Comparison of the (002) plane rocking curves; (**b**) the (002) plane FWHM and peak intensity shift; (**c**) comparison of the (102) plane rocking curves; (**d**) the (102) plane FWHM and peak intensity shift.

Furthermore, the circular transmission line model (CTLM) test demonstrates that the ohmic contact resistance (R_c) is reduced from 2.57 Ω·mm to 2.44 Ω·mm after NCD growth, as shown in Figure 6. Though this, the R_c is relatively large [36], the ohmic contact formation is confirmed, and its further optimizing will be carried out in the future to reduce this resistance.

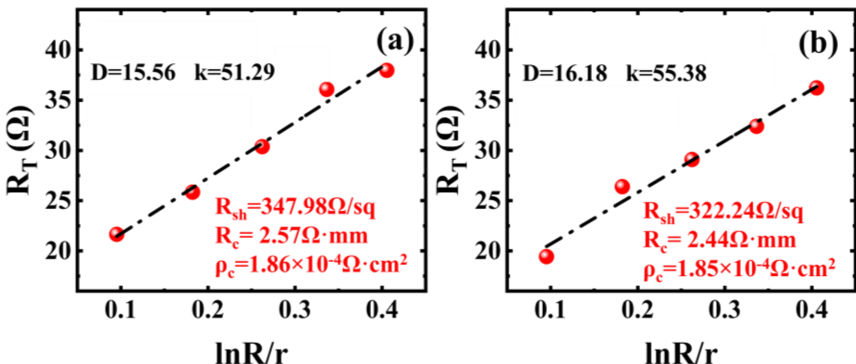

Figure 6. CTLM test results (**a**) before and (**b**) after NCD growth.

The DC output characteristics of devices with and without the NCD passivation layer are compared in Figure 7. Both devices have a gate length of 2 µm, a gate width of 100 µm, and source-drain and gate-drain distances of 19 µm and 14 µm, respectively. During the test, the drain-source voltage (V_{DS}) ranged from 0 to 15 V and the gate-source voltage (V_{GS}) varied from −5 to 4 V, with a voltage step of 1 V. As shown in Figure 7, the maximum saturation current (I_{Dmax}) of the device with the NCD passivation layer reaches 555 mA/mm at a gate voltage of 4 V. Compared with only 447 mA/mm for the device without NCD passivation, the obtained results indicate a 24% increase in I_{Dmax} due to the NCD passivation. The increase in current density is mainly due to the reduction in sheet and contact resistance. The on-resistance (R_{on}) of the device is reduced from 19.9 Ω·mm to 13.2 Ω·mm with NCD passivation, resulting in a reduction of approximately 34%. Additionally, under high-drain voltage conditions, the device with NCD passivation exhibits a smaller decrease in saturation current, further indicating that NCD passivation effectively suppresses the self-heating effect of the device [37]. It can also be observed that both devices show almost the same current density at V_{GS} = 0 V and V_{DS} = 10 V, with an output power density of around 2 W/mm. Although both devices own the same output power density, the junction temperature differs from each other (shown later in Figure 10), which is attributed to the introduction of NCD passivation, which enhances the heat dissipation performance.

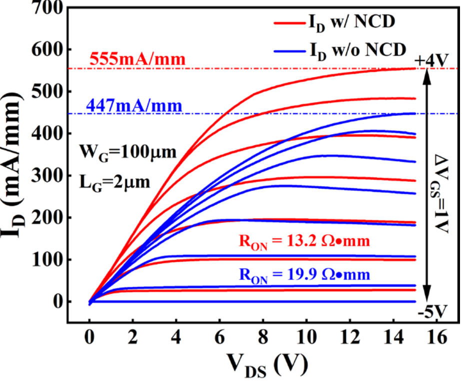

Figure 7. Output characteristics comparison between the devices with and without the NCD passivation layer.

The curves shown in Figure 8 present the transfer and transconductance (G_m) characteristics of devices with and without NCD passivation. The threshold voltage (Vth) of both devices is nearly equal, with the same value of −2.8 V. However, the peak transconductance ($G_{m,max}$) of the device with NCD passivation reaches 97.0 mS/mm, and it is 82.8 mS/mm for the device without NCD passivation.

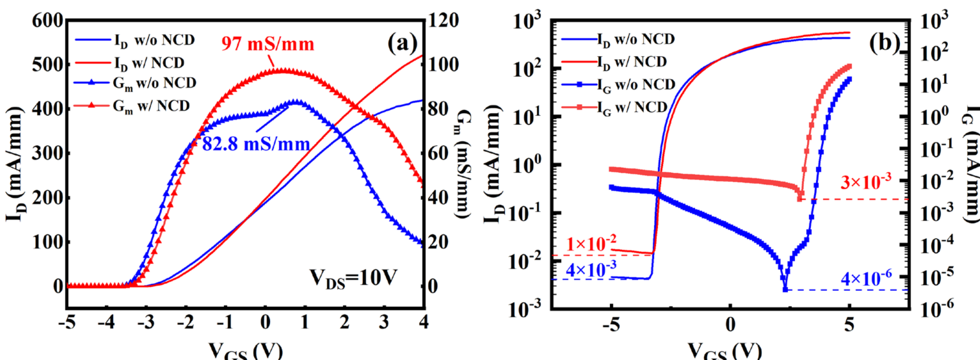

Figure 8. Transfer characteristics comparison between the devices with and without the NCD passivation layer. (**a**) I_D and G_m; (**b**) I_D and I_G.

Based on the R_C and R_{sheet} results, the source resistance of the devices with and without NCD passivation is 13.02 Ω and 12.12 Ω, respectively. The calculated intrinsic peak transconductance values are 109.9 mS/mm for the device with the NCD layer and 92.8 mS/mm for the device without it. The drain and gate leakage currents for the device with the NCD layer are 10^{-2} and 3×10^{-3} mA/mm, respectively. They are 4×10^{-3} and 4×10^{-6} mA/mm for the device without the NCD layer, respectively. After NCD passivation, the gate leakage current increased by three orders of magnitude, primarily due to the damage caused to the nitride surface by the two-step gate region ICP etching. This degradation can be reduced in the future by annealing the sample and optimizing the ICP etching process conditions [38].

The curves shown in Figure 9 present the breakdown characteristics of devices with and without NCD passivation. The off-state breakdown voltage (V_{br}) of the device with NCD is 500 V, which is 100 V higher than that of the device without NCD. The increase in breakdown voltage can be considered as the presence of the NCD passivation layer, which forms a T-shaped gate. This structure is beneficial for optimizing the electric field distribution around the gate region.

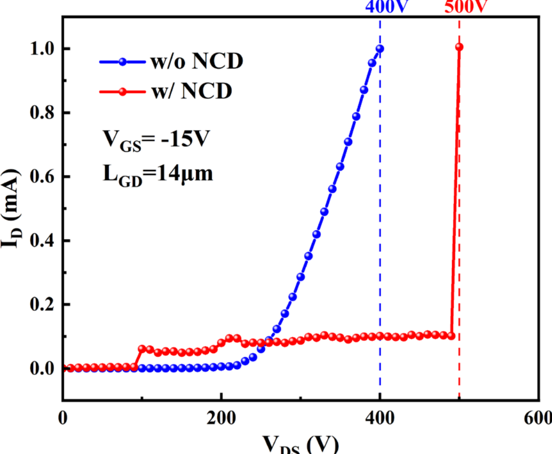

Figure 9. Breakdown characteristics comparison between the devices with and without the NCD passivation layer.

Finally, the thermal characteristics of devices with and without the NCD passivation layer were tested using a FOTRIC infrared thermal imaging system at room temperature. To accurately extract the junction temperature under high power, we use a device with a gate width of 1 mm. The source and gate of the devices were grounded, while the drain voltages were set to 5 V, 10 V, 15 V, and 20 V, respectively. The relationship between the output power density and junction temperature at different drain voltages is shown in Figure 10. It can be observed that the slopes of the junction temperature vs. output power density for the devices with and without NCD passivation are 16.38 °C/W·mm and 25.88 °C/W·mm, respectively, indicating a 36% improvement in heat dissipation efficiency after NCD passivation. From the summary in Table 1, it can be seen that, compared to the previous reports, the fabricated device with a NCD passivation layer in this work has significantly improved the heat dissipation efficiency [26–28,31]. These results clearly demonstrate the potential of NCD passivation for enhancing heat dissipation in GaN high-power devices.

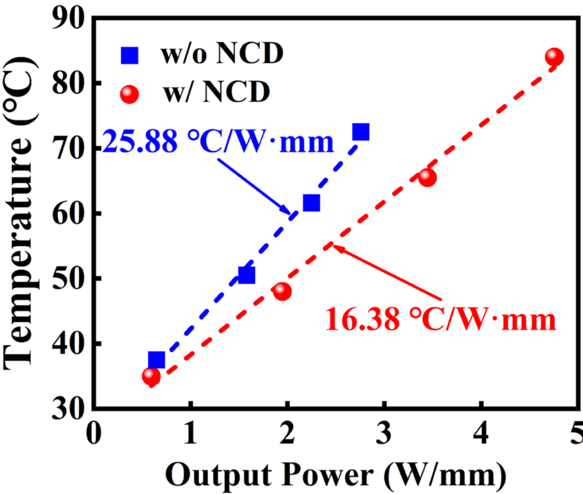

Figure 10. Junction temperature variations in the devices with and without the NCD passivation layer under different output power densities.

Table 1. Summary of the GaN HEMTs reports with NCD passivation.

Works	Substrate	Passivation Layer	I_{dmax} (mA/mm)	Heat Dissipation Improvement	V_{br} (V)
Ref. [31]	Si	50 nm SiO_2 + 500 nm NCD	249.6	~20%	140 V
Ref. [27]	SiC	50 nm SiN_x + 500 nm NCD	445	~20%	800 V
Ref. [28]	SiC	20 nm SiN_x + 500 nm NCD	743.28	21.4%	/
Ref. [26]	SiC	5 nm SiN_x + 500 nm NCD	1450	29.4%	/
This work	Si	50 nm SiN_x + 250–383 nm NCD	555	36%	500 V

4. Conclusions

In this study, the heat dissipation performance of AlGaN/GaN-on-Si HEMT devices was optimized using NCD passivation. Compared to the device without NCD passivation, the output current density of the NCD-passivated device increased by 24%. Moreover, R_{on} was reduced by 34.1%, and the degradation of current density caused by the self-heating effect was visibly suppressed. Additionally, the junction temperature test results under DC operation showed that the heat dissipation efficiency of the NCD-passivated device was optimized by 36%. These results show that NCD passivation can significantly reduce junction temperature and enhance the performance of GaN-based high-power devices.

Furthermore, it is compatible with the existing device fabrication process and is expected to play a crucial role in the future development of power electronic devices.

Author Contributions: Conceptualization, Z.R.; Methodology, Y.F.; Validation, J.C.; Formal analysis, L.Z.; Investigation, S.S. and L.Z.; Resources, Z.R., W.M., Y.H. and J.Z. (Jincheng Zhang); Data curation, S.S.; Writing—original draft, S.S.; Writing—review & editing, Y.F., Z.R. and J.Z. (Jinfeng Zhang); Supervision, Z.R. and J.Z. (Jinfeng Zhang); Project administration, J.L.; Funding acquisition, Y.F., Z.R., J.Z. (Jinfeng Zhang), K.S., J.C., T.Z. and W.Z. All authors have read and agreed to the published version of the manuscript.

Funding: Project supported by the Key Research and Development Plan of Shandong Province (Grant No. 2022CXGC020306), the National Natural Science Foundation of China (Grant Nos. 62127812, 62374122, 62134006, 62204193, 62404172), the Hefei Comprehensive National Science Center, the Key Research and Development Program of Anhui Province (Grant No. 2023a05020006), Xiaomi Young Scholar Funding, the Postdoctoral Science Foundation under (Grant No. 2021TQ0256), the Fundamental Research Funds for the Central Universities (Grant Nos. XJSJ24054, YJSJ24020).

Data Availability Statement: The original contributions presented in this study are included in the article. Further inquiries can be directed to the corresponding authors.

Conflicts of Interest: Author Weidong Man is employed by the company Shanghai Zhengshi Technology Co., Ltd. The remaining authors declare that the research was conducted in the absence of any commercial or financial relationships that could be construed as potential conflicts of interest.

References

1. Bader, S.J.; Lee, H.; Chaudhuri, R.; Huang, S.; Hickman, A.; Molnar, A.; Xing, H.G.; Jena, D.; Then, H.W.; Chowdhury, N.; et al. Prospects for Wide Bandgap and Ultrawide Bandgap CMOS Devices. *IEEE Trans. Electron Devices* **2020**, *67*, 4010–4020. [CrossRef]
2. Liu, X.; Zhang, S.; Wei, K.; Zhang, Y.; Yin, H.; Chen, X.; Huang, S.; Liu, G.; Zheng, Y.; Yuan, T.; et al. Improved Stability of GaN MIS-HEMT With 5-nm Plasma-Enhanced Atomic Layer Deposition SiN Gate Dielectric. *IEEE Electr. Device Lett.* **2022**, *43*, 1408–1411. [CrossRef]
3. Mazumder, S.K.; Voss, L.F.; Dowling, K.M.; Conway, A.; Hall, D.; Kaplar, R.J.; Pickrell, G.W.; Flicker, J.; Binder, A.T.; Chowdhury, S.; et al. Overview of Wide/Ultrawide Bandgap Power Semiconductor Devices for Distributed Energy Resources. *IEEE J. Emerg. Sel. Top. Power Electron.* **2023**, *11*, 3957. [CrossRef]
4. Mao, W.; Fan, J.-S.; Du, M.; Zhang, J.-F.; Zheng, X.-F.; Wang, C.; Ma, X.-H.; Zhang, J.-C.; Hao, Y. Analysis of the modulation mechanisms of the electric field and breakdown performance in AlGaN/GaN HEMT with a T-shaped field-plate. *Chin. Phys. B* **2016**, *25*, 127305. [CrossRef]
5. Su, C.-W.; Wang, T.-W.; Wu, M.-C.; Ko, C.-J.; Huang, J.-B. Fabrication and characterization of GaN HEMTs grown on SiC substrates with different orientations. *Solid-State Electron.* **2021**, *179*, 107980. [CrossRef]
6. Desai, N.; Then, H.W.; Yu, J.; Krishnamurthy, H.K.; Lambert, W.J.; Butzen, N.; Weng, S.; Schaef, C.; Radhakrishnan, K.; Ravichandran, K.; et al. A 32-A, 5-V-Input, 94.2% Peak Efficiency High-Frequency Power Converter Module Featuring Package-Integrated Low-Voltage GaN nMOS Power Transistors. *IEEE J. Solid-State Circuits* **2022**, *57*, 1090–1099. [CrossRef]
7. Chen, J.; Peng, H.; Feng, Z.; Kang, Y. A GaN BCM AC–DC Converter for Sub-1 V Electromagnetic Energy Harvesting With Enhanced Output Power. *IEEE Trans. Power Electron.* **2021**, *36*, 9285–9299. [CrossRef]
8. Malakoutian, M.; Kasperovich, A.; Rich, D.; Woo, K.; Perez, C.; Soman, R.; Saraswat, D.; Kim, J.-k.; Noshin, M.; Chen, M.; et al. Cooling future system-on-chips with diamond inter-tiers. *Cell Rep. Phys. Sci.* **2023**, *4*, 101686. [CrossRef]
9. Malakoutian, M.; Laurent, M.A.; Chowdhury, S. A Study on the Growth Window of Polycrystalline Diamond on Si3N4-coated N-Polar GaN. *Crystals* **2019**, *9*, 498. [CrossRef]
10. Minoura, Y.; Ohki, T.; Okamoto, N.; Sato, M.; Ozaki, S.; Yamada, A.; Kotani, J. GaN MMICs on a diamond heat spreader with through-substrate vias fabricated by deep dry etching process. *Appl. Phys. Express* **2022**, *15*, 036501. [CrossRef]
11. Qin, Y.; Albano, B.; Spencer, J.; Lundh, J.S.; Wang, B.; Buttay, C.; Tadjer, M.; DiMarino, C.; Zhang, Y. Thermal management and packaging of wide and ultra-wide bandgap power devices: A review and perspective. *J. Phys. D Appl. Phys* **2023**, *56*, 093001. [CrossRef]
12. Malakoutian, M.; Ren, C.; Woo, K.; Li, H.; Chowdhury, S. Development of Polycrystalline Diamond Compatible with the Latest N-Polar GaN mm-Wave Technology. *Cryst. Growth Des.* **2021**, *21*, 2624–2632. [CrossRef]

13. Angadi, M.A.; Watanabe, T.; Bodapati, A.; Xiao, X.; Auciello, O.; Carlisle, J.A.; Eastman, J.A.; Keblinski, P.; Schelling, P.K.; Phillpot, S.R. Thermal transport and grain boundary conductance in ultrananocrystalline diamond thin films. *J. Appl. Phys.* **2006**, *99*, 114301. [CrossRef]
14. Tadjer, M.J.; Anderson, T.J.; Ancona, M.G.; Raad, P.E.; Komarov, P.; Bai, T.; Gallagher, J.C.; Koehler, A.D.; Goorsky, M.S.; Francis, D.A.; et al. GaN-On-Diamond HEMT Technology With TAVG = 176 °C at PDC,max = 56 W/mm Measured by Transient Thermoreflectance Imaging. *IEEE Electr. Device Lett.* **2019**, *40*, 881–884. [CrossRef]
15. Wu, M.; Zhang, X.; Yang, L.; Ma, X.; Hao, Y. Noninvasive Lift-off Technology for Integration of GaN HEMTs with Diamond. In Proceedings of the 6th IEEE Electron Devices Technology & Manufacturing Conference (EDTM), Oita, Japan, 6–9 March 2022; pp. 122–124.
16. Gerrer, T.; Cimalla, V.; Waltereit, P.; Müller, S.; Benkhelifa, F.; Maier, T.; Czap, H.; Ambacher, O.; Quay, R. Transfer of AlGaN/GaN RF-devices onto diamond substrates via van der Waals bonding. *Int. J. Microw. Wirel. Technol.* **2018**, *10*, 666–673. [CrossRef]
17. Gerrer, T.; Pomeroy, J.; Yang, F.; Francis, D.; Carroll, J.; Loran, B.; Witkowski, L.; Yarborough, M.; Uren, M.J.; Kuball, M. Thermal Design Rules of AlGaN/GaN-Based Microwave Transistors on Diamond. *IEEE Trans. Electron Devices* **2021**, *68*, 1530. [CrossRef]
18. Gohel, K.; Zhou, L.; Mukhopadhyay, S.; Pasayat, S.S.; Gupta, C. Understanding of multiway heat extraction using peripheral diamond in an AlGaN/GaN high electron mobility transistor by electrothermal simulations. *Semicond. Sci. Technol.* **2024**, *39*, 075016. [CrossRef]
19. Gu, Y.; Zhang, Y.; Hua, B.; Ni, X.; Fan, Q.; Gu, X. Interface Engineering Enabling Next Generation GaN-on-Diamond Power Devices. *J. Electron. Mater.* **2021**, *50*, 4239–4249. [CrossRef]
20. Ren, Z.; Xu, J.; Le, X.; Lee, C. Heterogeneous Wafer Bonding Technology and Thin-Film Transfer Technology-Enabling Platform for the Next Generation Applications beyond 5G. *Micromachines* **2021**, *12*, 946. [CrossRef]
21. Wang, Y.; Hu, X.; Ge, L.; Liu, Z.; Xu, M.; Peng, Y.; Li, B.; Yang, Y.; Li, S.; Xie, X.; et al. Research Progress in Capping Diamond Growth on GaN HEMT: A Review. *Crystals* **2023**, *13*, 946. [CrossRef]
22. Liang, J.; Kobayashi, A.; Shimizu, Y.; Ohno, Y.; Kim, S.W.; Koyama, K.; Kasu, M.; Nagai, Y.; Shigekawa, N. Fabrication of GaN/Diamond Heterointerface and Interfacial Chemical Bonding State for Highly Efficient Device Design. *Adv. Mater.* **2021**, *33*, 2104564. [CrossRef] [PubMed]
23. Matsumae, T.; Kurashima, Y.; Takagi, H.; Shirayanagi, Y.; Hiza, S.; Nishimura, K.; Higurashi, E. Room temperature bonding of GaN and diamond substrates via atomic layer. *Scr. Mater.* **2022**, *215*, 114725. [CrossRef]
24. Mu, F.; Xu, B.; Wang, X.; Gao, R.; Huang, S.; Wei, K.; Takeuchi, K.; Chen, X.; Yin, H.; Wang, D.; et al. A novel strategy for GaN-on-diamond device with a high thermal boundary conductance. *J. Alloys Compd.* **2022**, *905*, 164076. [CrossRef]
25. Hu, X.; Ge, L.; Liu, Z.; Li, M.; Wang, Y.; Han, S.; Peng, Y.; Xu, M.; Hu, X.; Tang, G.; et al. Diamond-SiC composite substrates: A novel strategy as efficient heat sinks for GaN-based devices. *Carbon* **2024**, *218*, 118755. [CrossRef]
26. Soman, R.; Malakoutian, M.; Shankar, B.; Field, D.; Akso, E.; Hatui, N.; Hines, N.J.; Graham, S.; Mishra, U.K.; Kuball, M.; et al. Novel all-around diamond integration with GaN HEMTs demonstrating highly efficient device cooling. In Proceedings of the 2022 International Electron Devices Meeting (IEDM), San Francisco, CA, USA, 3–7 December 2022; pp. 30.38.31–30.38.34.
27. Anderson, T.J.; Hobart, K.D.; Tadjer, M.J.; Koehler, A.D.; Imhoff, E.A.; Hite, J.K.; Feygelson, T.I.; Pate, B.B.; Eddy, C.R.; Kub, F.J. Nanocrystalline Diamond Integration with III-Nitride HEMTs. *ECS J. Solid State Sci. Technol.* **2016**, *6*, Q3036–Q3039. [CrossRef]
28. Guo, H.; Li, Y.; Yu, X.; Zhou, J.; Kong, Y. Thermal Performance Improvement of AlGaN/GaN HEMTs Using Nanocrystalline Diamond Capping Layers. *Micromachines* **2022**, *13*, 1486. [CrossRef]
29. Ryou, J.-H.; Choi, S. All-around diamond for cooling power devices. *Nat. Electron.* **2022**, *5*, 834. [CrossRef]
30. Zhou, X.; Malakoutian, M.; Soman, R.; Bian, Z.; Martinez, R.P.; Chowdhury, S. Impact of Diamond Passivation on fT and fmax of mm-wave N-Polar GaN HEMTs. *IEEE Trans. Electron Devices* **2022**, *69*, 6650. [CrossRef]
31. Tadjer, M.J.; Anderson, T.J.; Hobart, K.D.; Feygelson, T.I.; Caldwell, J.D.; Eddy, C.R.; Kub, F.J.; Butler, J.E.; Pate, B.; Melngailis, J. Reduced Self-Heating in AlGaN/GaN HEMTs Using Nanocrystalline Diamond Heat-Spreading Films. *IEEE Electr. Device Lett.* **2012**, *33*, 23–25. [CrossRef]
32. Babchenko, O.; Dzuba, J.; Lalinský, T.; Vojs, M.; Vincze, A.; Ižák, T.; Vanko, G. Stability of AlGaN/GaN heterostructures after hydrogen plasma treatment. *Appl. Surf. Sci.* **2017**, *395*, 92–97. [CrossRef]
33. Xu, T.; Yang, S.; Lu, J.; Xue, Q.; Li, J.; Guo, W.; Sun, Y. Characterization of nanocrystalline diamond films implanted with nitrogen ions. *Diam. Relat. Mater.* **2001**, *10*, 1441–1447. [CrossRef]
34. Ferrari, A.C.; Robertson, J. Origin of the1150−cm−1Raman mode in nanocrystalline diamond. *Phys. Rev. B* **2001**, *63*, 121405. [CrossRef]
35. Tian, Y.; Ma, H.A.; Li, S.S.; Xiao, H.Y.; Zhang, Y.F.; Huang, G.F.; Ma, L.Q.; Jia, X.P. Dependence of limited growth rate of high-quality gem diamond on growth conditions. *Chin. Phys. Lett.* **2007**, *24*, 2115–2117.
36. Greco, G.; Iucolano, F.; Roccaforte, F. Ohmic contacts to Gallium Nitride materials. *Appl. Surf. Sci.* **2016**, *383*, 324–345. [CrossRef]

37. Benbakhti, B.; Soltani, A.; Kalna, K.; Rousseau, M.; De Jaeger, J.-C. Effects of Self-Heating on Performance Degradation in AlGaN/GaN-Based Devices. *IEEE Trans. Electron Devices* **2009**, *56*, 2178–2185. [CrossRef]
38. Conroy, M.; Li, H.; Zubialevich, V.Z.; Kusch, G.; Schmidt, M.; Collins, T.; Glynn, C.; Martin, R.W.; O'Dwyer, C.; Morris, M.D.; et al. Self-Healing Thermal Annealing: Surface Morphological Restructuring Control of GaN Nanorods. *Cryst. Growth Des.* **2016**, *16*, 6769–6775. [CrossRef]

Disclaimer/Publisher's Note: The statements, opinions and data contained in all publications are solely those of the individual author(s) and contributor(s) and not of MDPI and/or the editor(s). MDPI and/or the editor(s) disclaim responsibility for any injury to people or property resulting from any ideas, methods, instructions or products referred to in the content.